Trends in advanced sciences and technology

Trends in Advanced Sciences and Technology

Manuscript 1007

Integration of 3D Structural Modelling and Well Logging Analysis in the Evaluation Of October Oil field, Gulf of Suez, Egypt

Lamiaa Yahia

Mostafa Toni

Farouk I. Metwalli

M. H. Mansour

Amir Ismail

ORIGINAL STUDY

Integration of Three Dimensional Structural Modelling and Well Logging Analysis in the Evaluation of October Oil Field, Gulf of Suez, Egypt

Lamiaa Yahia [a], Mostafa Toni [a,b], Farouk I. Metwalli [a], M.H. Mansour [c], Amir Ismail [a,d,*]

[a] Department of Geology, Faculty of Science, Helwan University, Egypt
[b] National Program for Earthquakes and Volcanoes, Geohazard Center, Saudi Geological Survey, Jeddah, Saudi Arabia
[c] Gulf of Suez Petroleum Company, New Maadi, Cario, Egypt
[d] Department of Physical and Environmental Sciences, Texas A and M University, Corpus Christi, TX, USA

Abstract

An extensive study of the NUBIA and MAT reservoirs, incorporating numerous data sources, enhances the accuracy of production forecasts for hydrocarbon exploration and development. This study aims to integrate seismic and well data for re-assessment and to delineate the geological and petrophysical characteristics of the October oil field which is one of the most productive in the central Gulf of Suez, but it has recently witnessed a drop in output in some regions, and some wells have begun to depletion. While facies modeling enabled the spatial distribution of lithologic facies inside the constructed three-dimensional (3D) structural model, which reflected two types of facies: marine carbonates and lagoon shale, petrophysical analysis described the whole distribution of petrophysical features. The incorporation of described structures, horizons, and selected zones for 3D grid express northwest-southwest fault systems governs structural modeling. This study focuses on the structural components of this vast field in order to update its structural model with high-resolution 2D seismic lines and well logs. The discovered reservoir possesses favorable reservoir characteristics that will increase hydrocarbon production in this field (low net pay, low effective porosity, low shale content, and high water saturation). The structural set is assumed to be in charge of the October oil field's petrophysical discoveries and facies distribution. The models demonstrate the effects of structural features and their control over the interpretation of reservoirs' facies and petrophysical properties. The region is tectonically affected by a large normal fault (NE-SW) with large displacement, followed by small normal and reverse faults that may be the reason for the presence of traps. The extracted 3D structural model and cross-sections indicate faults in the region.

Keywords: Three dimensional structural modelling, Gulf of suez, October oil field, Seismic interpretation, Well logging

1. Introduction

The Gulf of Suez formed in the estimated 26 million-year-old, dormant Gulf of Suez Rift basin. It is approximately 300 kg (190 miles) long and finishes at the Suez Canal's entrance and the Egyptian city of Suez. The Gulf's core is divided by the African-Asian divide (Awni et al., 1990).

October Field is the largest oil field in the Gulf of Suez Rift basin, draining over 8000 acres (3238 ha) with 20 wells from five platforms in about 190 feet (58 m) of water. It is the third-largest oil field in Egypt, producing 378 million barrels of oil from its discovery in 1977 until January 1990. Successful field extensions in recent years show that it is worthwhile to continue exploring this oil-rich region (Lelek et al., 1992). The tectonic and structural settings of the Gulf have been studied recently employing various geophysical tools including aeromagnetic data (Zahra and Nakhla, 2016), integration of seismic and petrophysical analysis (Gawad et al., 2021),

Received 30 January 2024; revised 5 April 2024; accepted 11 April 2024.
Available online 28 May 2024

* Corresponding author at: Department of Physical and Environmental Sciences, Texas A and M University, 6300 Ocean Drive, Corpus Christi, TX 78412, USA.
E-mail addresses: amir_ismail@science.helwan.edu.eg, amir.ismail@tamucc.edu (A. Ismail).

https://doi.org/10.62537/2974-444X.1007

and three dimensional (3D) seismic modelling of complex structural reservoirs (Sercombe et al., 2012; Khattab et al., 2023).

The rotating fault blocks that make up this structurally confined field are common to all rift basins globally. A northwest-trending normal fault with an approximate throw of 4000 feet (1220 m) is trapping an oil column that extends 1110 feet (335 m) on the upthrown eastern side. The uplifted side's pre-rift section from the Carboniferous to the Oligocene slopes gently to the northeast. It is covered in clastics, carbonates, and evaporites that are not uniformly flat from the Miocene to the Holocene. Thick Miocene evaporites obstructing seismic characterization of the highly productive pre-rift area providing severe and numerous issues. These same evaporites provide the final seal in October Field and throughout the Gulf of Suez. Approximately 95% of field reserves are found in the huge Nubia Sandstones of the Carboniferous to Lower Cretaceous era, despite the fact that four levels are productive (Halbouty, 1992).

The thick Miocene South Gharib and Belayim layers provide seismic reflection multiples that conceal the reflections of the underlying reservoirs (Badri et al., 1999). The study site is in the Gebel El-Zeit region, which is located on the Gulf of Suez's southwest shore. The Ras El Ush oil field is 80 km north of Hurghada City, 1.5 km east of the saddle between the large Gebel El Zeit and the little Zeit (Badri et al., 1999).

The aim of this study, October oil field suffered a lack of production in some areas, in addition to some wells that have begun to deplete, which negatively affects the economic value of this field, 3D modeling helps to achieve the aim of the study as follows:

(a) Enhance the estimation of the reserve's potential and capability to make decisions.
(b) Create a new 3D structural model that highlights the key structural features associated with the computed petrophysical analysis, allowing for an evaluation of the geological and petrophysical characteristics in the study area.
(c) Identify new prospects based on 3D modeling, petrophysical analysis, and the petroleum system in the region.

To fulfill these objectives, twenty 2D seismic lines, check shots, and well log data from four wells were used for petrophysical analysis and to construct a 3D structural model (Fig. 1).

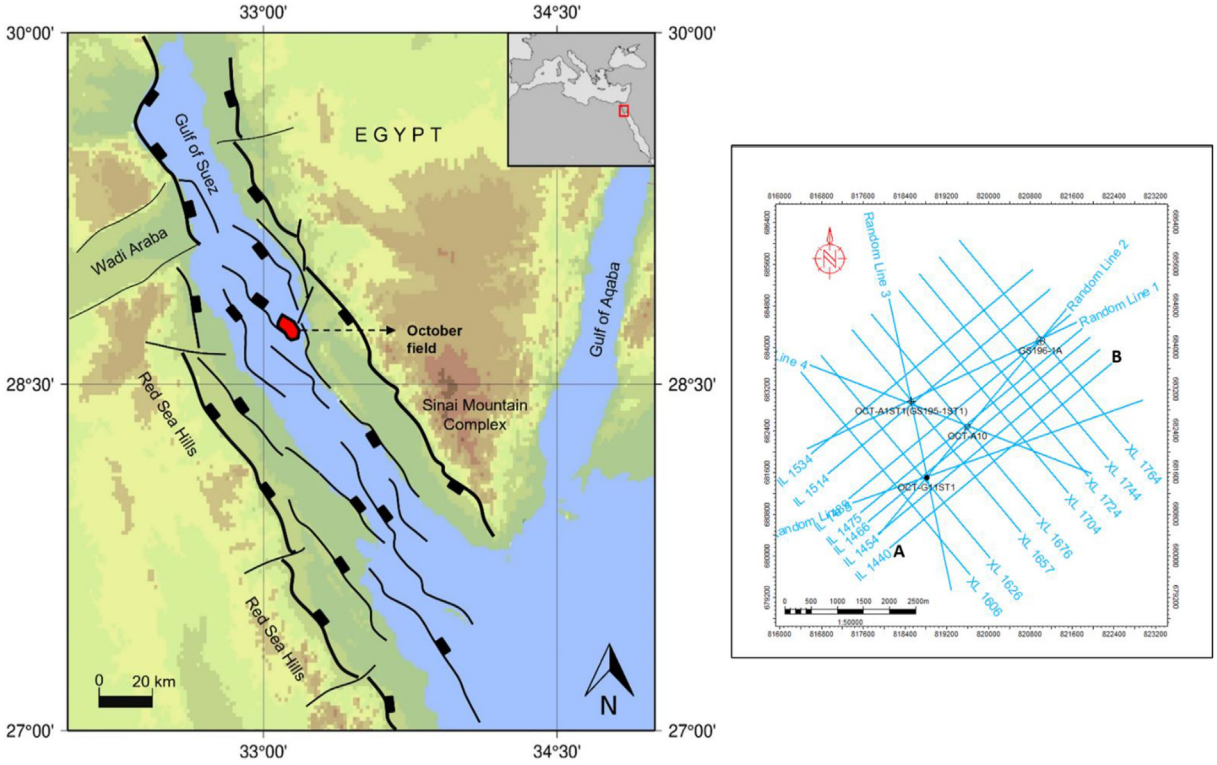

Fig. 1. Location map of the October oil field, Gulf of Suez, Egypt (left) (El-Gendy et al., 2017), illustrating the accessible seismic lines and studied wells in the study area (right).

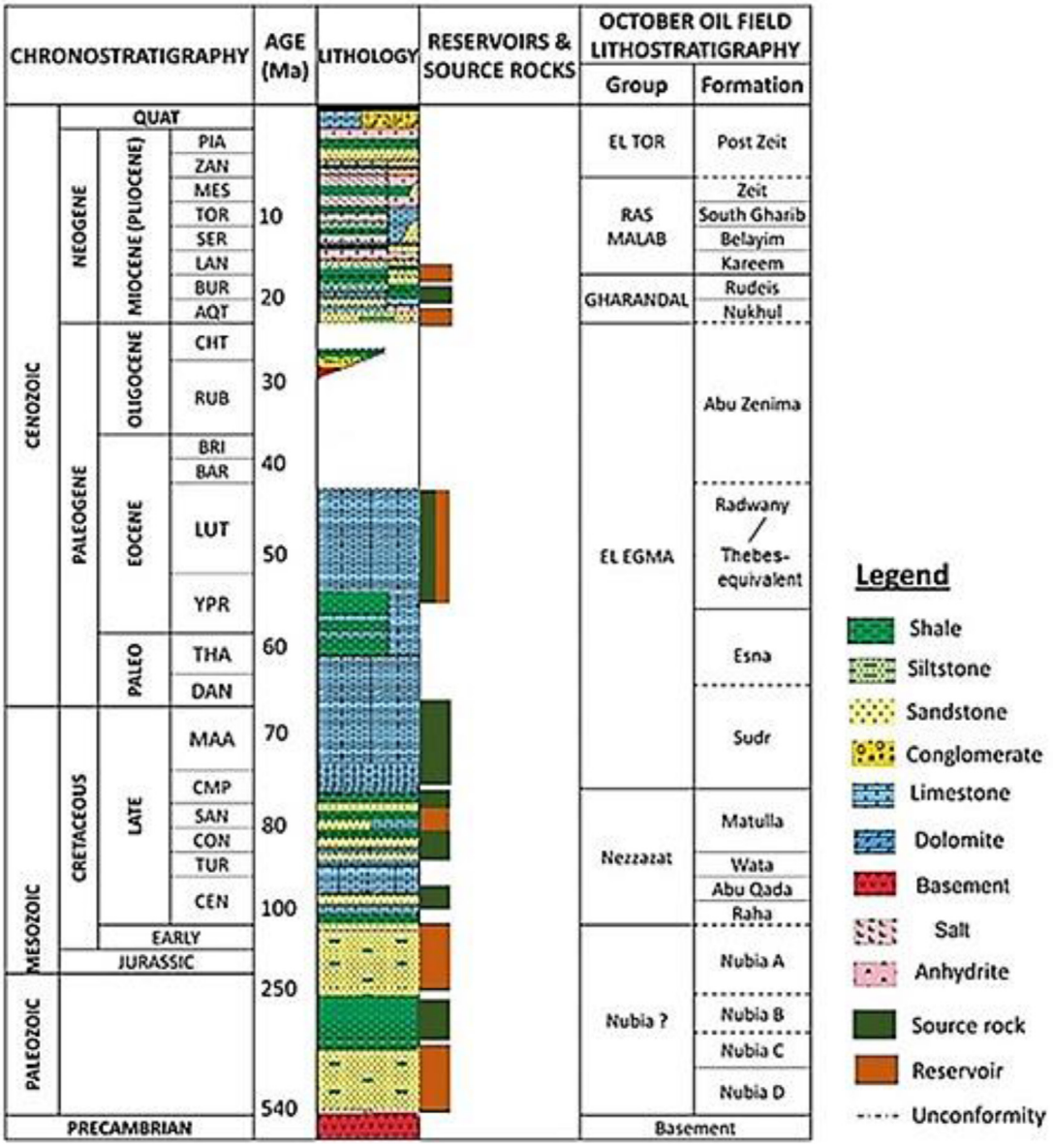

Fig. 2. Stratigraphy of the October oil Field, showing generalized lithologies and thicknesses (after Radwan et al., 2022). Abbreviations: AQT, Aquitanian; BAR, Bartonian; BUR, Burdigalian; CEN, Cenomanian; CHT, Chattian; CMP, Campanian; CON, Coniacian; DAN, Danian; LAN, Langhian; LUT, Lutetian; MAA, Maastrichtian; MES, Messinian; PIA is Piacenzian; PRI, Priabonian; RUP, Rupelian; SAN, Santonian; SER, Serravallian; THA, Thanetian; TOR, Tortonian; TUR, Turonian; YPR, Ypresian; ZAN, Zanclea.

2. Geological setting

2.1. Stratigraphic setting and structural setting

The tectonic evolution of the Gulf of Suez rift has had a profound impact on sedimentation. There are three recognized tectono-stratigraphic regimes: The pre-rift megasequence, which is located over the Pre-Cambrian basement, is made up of marine mudstones and carbonates from the Palaeozoic–Eocene, Mesozoic mixed continental and marginal marine strata (Triassic–Cretaceous), and Palaeozoic siliciclastics and volcanic (Carboniferous–Permian) (El-Tarabili and Adawy, 1972). During the early Oligocene, there was uplift and erosion. Between the late Oligocene and the Holocene, syn-rift and post-rift sedimentation occurred, resulting in the deposition of up to 3.5 km of marine and non-marine coastal sediments (El Sawi, 1985).

A sequence of significant extensional faults that strike in an NNW-SSE direction and follow the Clysmic trend define the Gulf of Suez. There are also recognized minor crossfaults regulated by basements (Patton et al., 1994; Montenat et al., 1998).

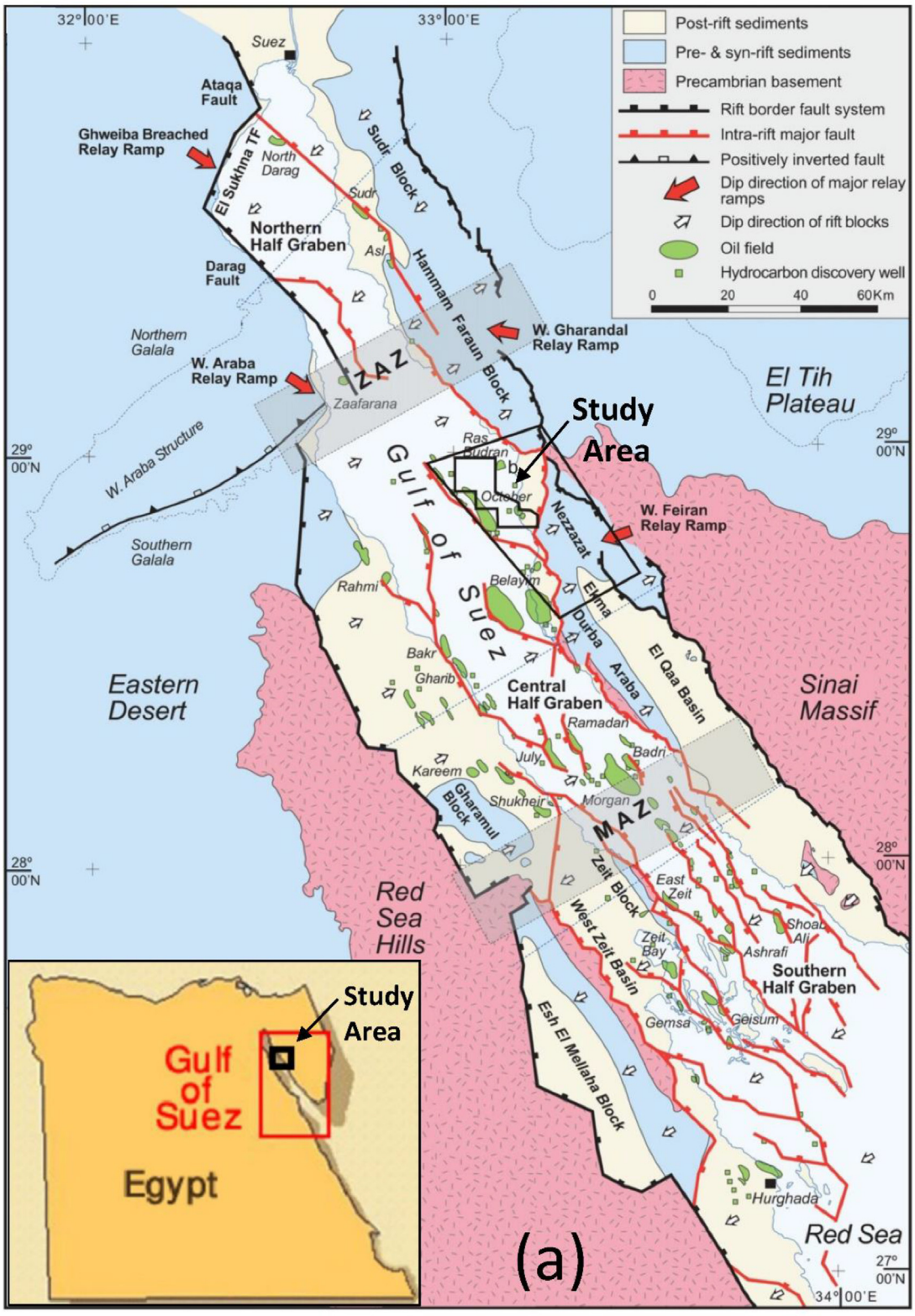

Fig. 3. Gulf of Suez rift tectonic map (Moustafa and Khalil 2020).

Table 1. Show the acquired wireline dataset company name, depth interval, and rate of record.

1-Company name
Owner: GUPCO
2-Depth interval
GS196-1A: 414–12547
OCT_A-1ST1: 1032–13235
OCT_G-11ST1: 8967–12031
OCT_A-10: 6691–12188
3-The rate of recorded
Quarter meter

This fault has produced massive, widely spaced (10–20 km) fault blocks with eroded crests, defining the rift's cross-sectional structure (Farhoud, 2009).

The October field is situated around 25 km north of the massive Belayim field. Its structure is made up of several long, NE-dipping, NW-SE-trending pre-Miocene faulted blocks that stretch for about 20 km along the strike (Zahran, 1986; EGPC, 1996). Several significant normal faults that descend to the west surround it to the west. Along with other smaller, tipped fault-block compartments, the field is split into two main blocks: the southern block and the subordinate northern block. Sediments from the Miocene and post-Miocene envelop the pre-Miocene structure. This field's structural axis runs parallel to October's. In contrast, the Ras Budran field, located ~15 km to the northeast, constitutes a distinct structural feature within the Gulf of Suez due to its composition of faulted blocks that dip and trend NE-SW (Chowdhary and Taha, 1987), as shown in Fig. 3.

3. Dataset and methods

3.1. Dataset

Static reservoir modeling precisely defines the reservoir's framework (geometry) and architecture (property). The current study investigated reservoir geometry (stratigraphy and structure) and petrophysical properties using the available data, which is: four wells with depth interval [GS196–1A (414–12547 ft), OCT_A–1ST1 (1032–13235 ft), OCT_G–11ST1 (8967–12031 ft), and OCT_A–10 (6691–12188 ft)] whose importance lies in analyzing petrophysical data for use in identifying lithology, determining hydrocarbons, and making seismic-well tie with interpreted stratigraphic tops and twenty 2D seismic lines, check shots, and well log data measured by GUPCO and rate of record quarter meter (Table 1) (resistivity, SP, GR, density, neutron, and sonic) (Fig. 4).

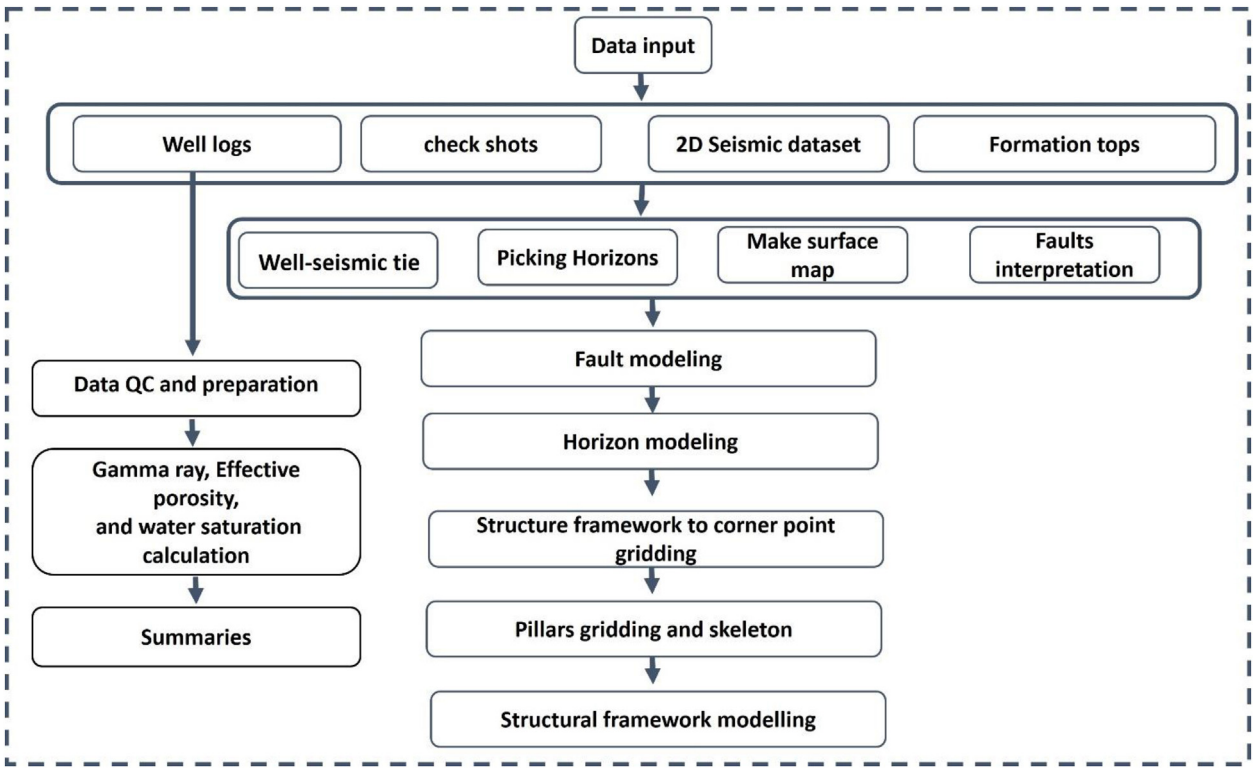

Fig. 4. Flowchart outlining the steps of the structural framework modeling.

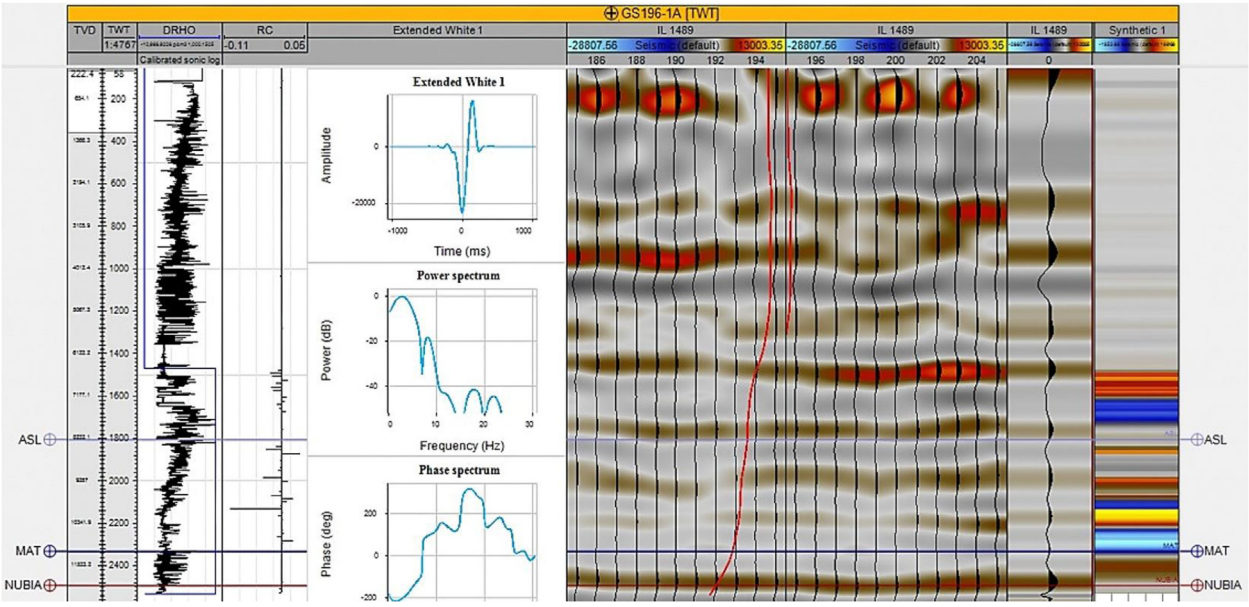

Fig. 5. Synthetic seismogram of well GS196-1A was generated for perfect correlation and tie with seismic data.

3.2. Seismic interpretation

The structural setting, which reflects the hydrocarbon traps (El Redini et al., 2017; Ismail et al., 2023), has a considerable influence on seismic data interpretation. Several seismic sections were developed to better understand the geologic basis (stratigraphic and structural) of the October field.

There is a possibility that one or more of these geologic formations are linked to the accumulation of hydrocarbons. This reduces the likelihood of drilling an unsuccessful exploratory well. As a result, the seismic data interpretation strategy for subsurface mapping is considered the most important interpretation step for mapping hydrocarbon structural traps.

The integration of seismic data with wireline logs (Fig. 5), achieved through the use of a one-dimensional synthetic seismogram, facilitates the identification of seismic occurrences (reflections) that correspond to geological formations, thereby establishing a connection between individual seismic reflectors and their respective stratigraphic markers (Badley, 1985; Zouaghi et al., 2011; Abdel-Fattah et al., 2015; Khan et al., 2019; Abdelwahhab and Raef, 2020; Ismail et al., 2020a).

The following equation was multiplied with density and sonic logs during the seismic-well tie operation to determine acoustic impedance.

$$Z = \rho V \tag{1}$$

$$V = \sqrt{\left(\frac{E}{\rho}\right)} \tag{2}$$

Where,

Z: acoustic impedance, V: acoustic velocity, ρ: density, and E: Elastic modulus.

Additionally, the results of the check shots survey improved the seismic tying and well. Because downhole data has a substantially larger frequency (Paulsson et al., 2001).

Keeping this in view synthetic seismogram is generated on minimum phase, Source depth 7.5 m Ricker wavelet of 12–8 HZ, *P*/B ratio 16, Str. N10 m, Peak-peak 120.4 barm, and normal polarity (Increase in impedance represented as peak) (Table 2) to achieve best seismic to well tie. Once the data was imported, the well logs were correlated to the seismic data. This ties horizons within the well logs and then correlates these to the seismic data using

Table 2. Show acquired seismic dataset company name, the type of migration, and physical parameters such as phase, and polarity.

1-Company name
Owner: GUPCO (1992)
Contractor: Geo team exploration Ltd. SA Norway
2-Phase
Minimum phase wavelet
3-Polarity
SEG normal polarity
An increase in impedance represented as a peak
4-Type of migration
Prestack depth migration

the checkshot information. This step was important in ensuring that the well and seismic data were accurately tied together for precise structural and stratigraphic analysis (Khan et al., 2019; Ismail et al., 2020b; El Dally et al., 2023) (Fig. 5).

Using Petrel software to pick and map formation tops for source, reservoir, and seal formations, THBES and BRLS were chosen as source formations. ASL, HAWARA, MAT, and NUBIA were selected as reservoirs. SGH and BABA were chosen as seal layers. Identified structural setting by geological faults picking such as F1, F2, F3, F4, and F5, which aid in the detection of traps that may exist in the study area, as depicted in Fig. 6.

In the second stage (Fig. 4), after picking horizons in time domain, create TWT structural contour maps for reservoir formation tops MAT and NUBIA (Figs. 7 and 8).

Applied the seismic phantom horizon interpretation approach in this study, which constructs a horizon on a reflection profile by averaging the dips of the reflections within a band. As a result, the dip's tendency is apparent; however, it may or may not coincide with a real boundary plane.

Creating a three-dimensional reservoir grid model is a crucial intermediate step that has a big impact on the geostatistics-based numerical simulation and reservoir property modeling that come next. The gridding method in geostatistical reservoir modelling fundamentally establishes how to quantify the reservoir's macroscopic homogeneity. When applying geostatistics to logical grids, a grid with the extreme and significant distortion can easily produce a distorted variogram, which can jeopardise the accuracy and dependability of modelling parameters like pore permeability and sedimentary facies Hoffman et al., 2006.

The pillar gridding 'Key Pillars' process generates the structural model, and the grid provides a framework for the modeling. Using Pillars to

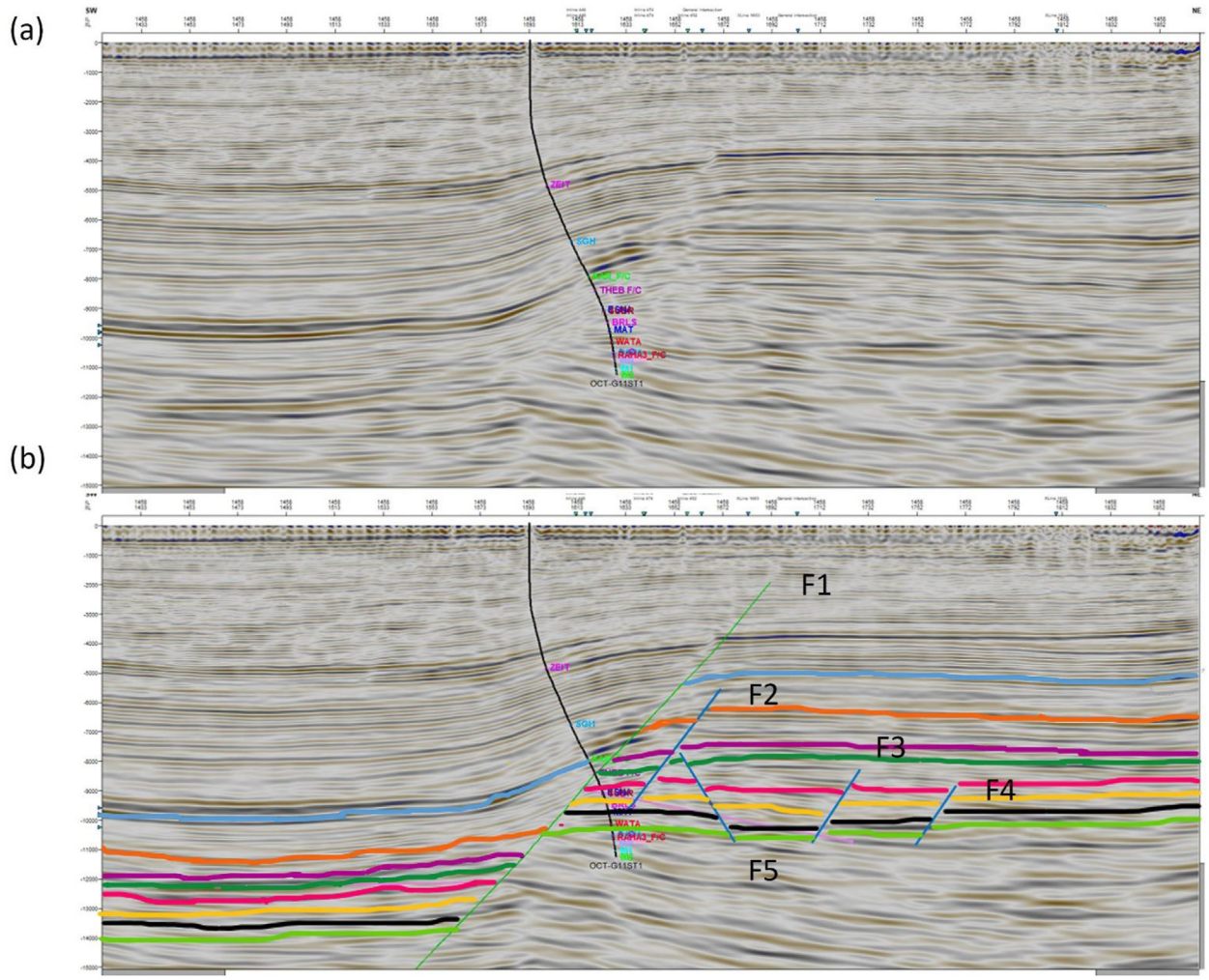

Fig. 6. Line IL 1440 (a) before and (b) after picking horizon and fault (see the location in Fig. 1).

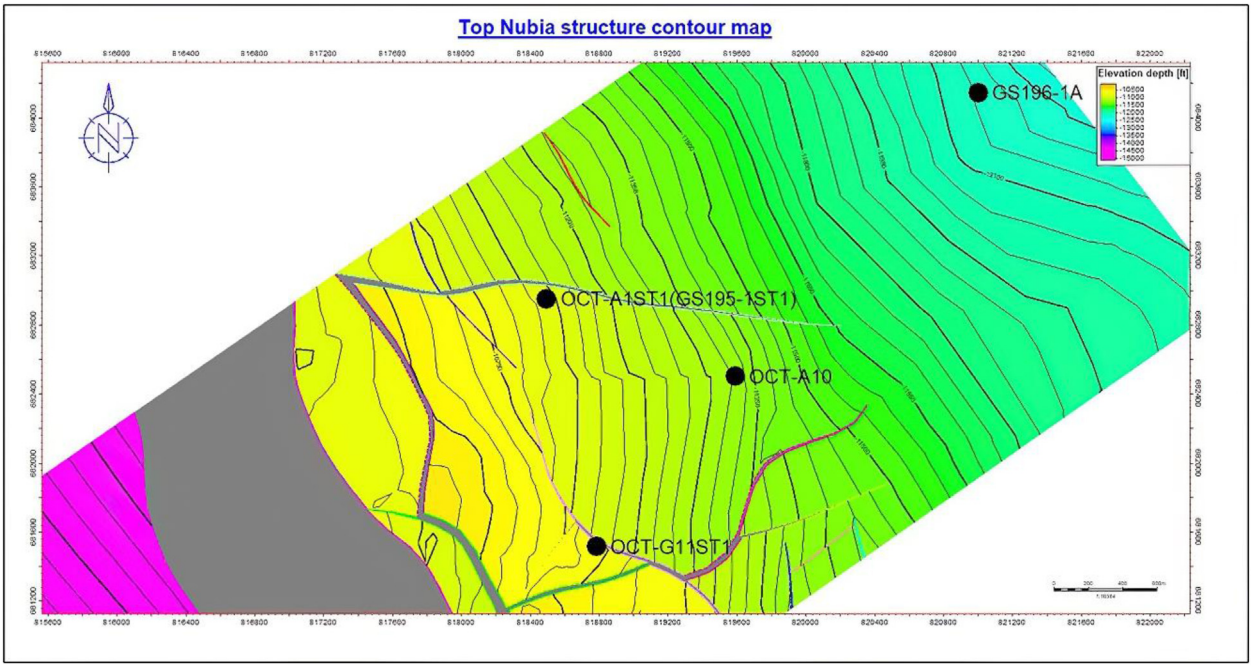

Fig. 7. Surface contour map of NUBIA formation.

construct fault planes in terms of length, form, azimuth, and dip in the 3D grid model and characterizing the fault in the geological model. The pillar gridding approach creates the structural model, and the grid provides a foundation for modeling.

Geophysicists frequently utilize pillar grids, with the corner point grid being the most prevalent type (Fig. 9). In terms of fault position, the pillar that directs the grid cells is parallel to the fault lines (Thom and Hocker, 2009).

Finally, generate the 3D seismic model using the picked horizons, faults, and TWT maps. The 3D seismic model provides the foundation for analyzing numerical models of reservoirs, physical

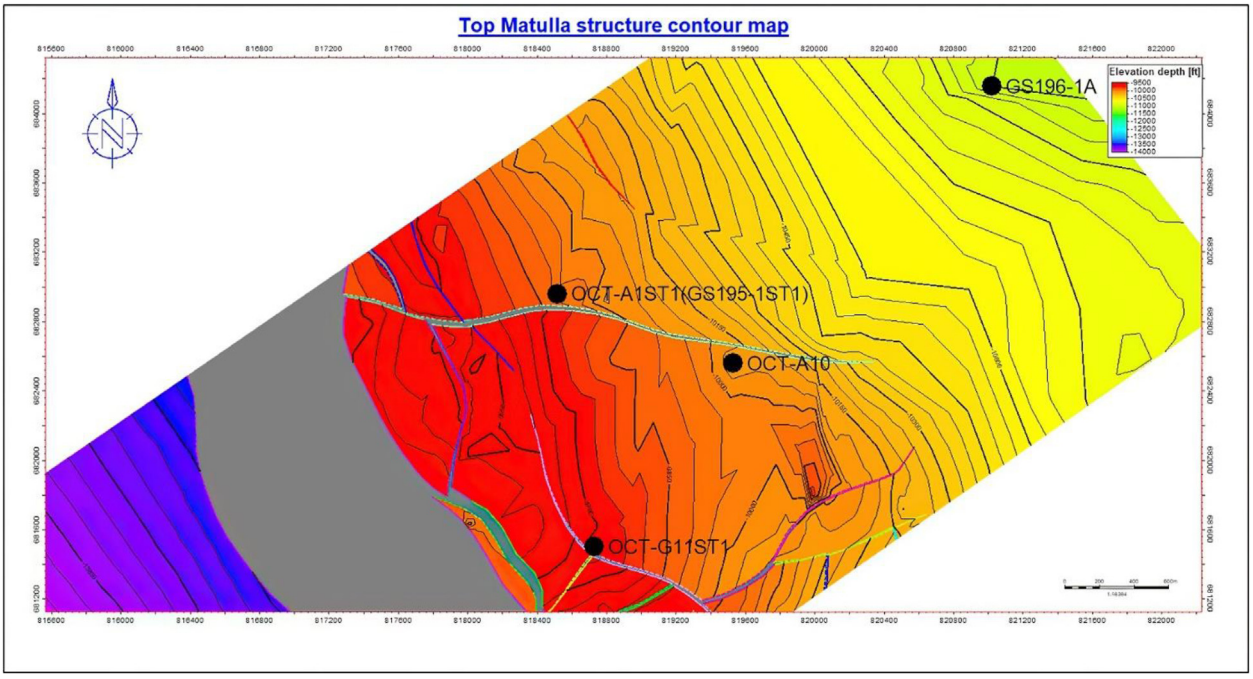

Fig. 8. Surface contour map of Matulla formation.

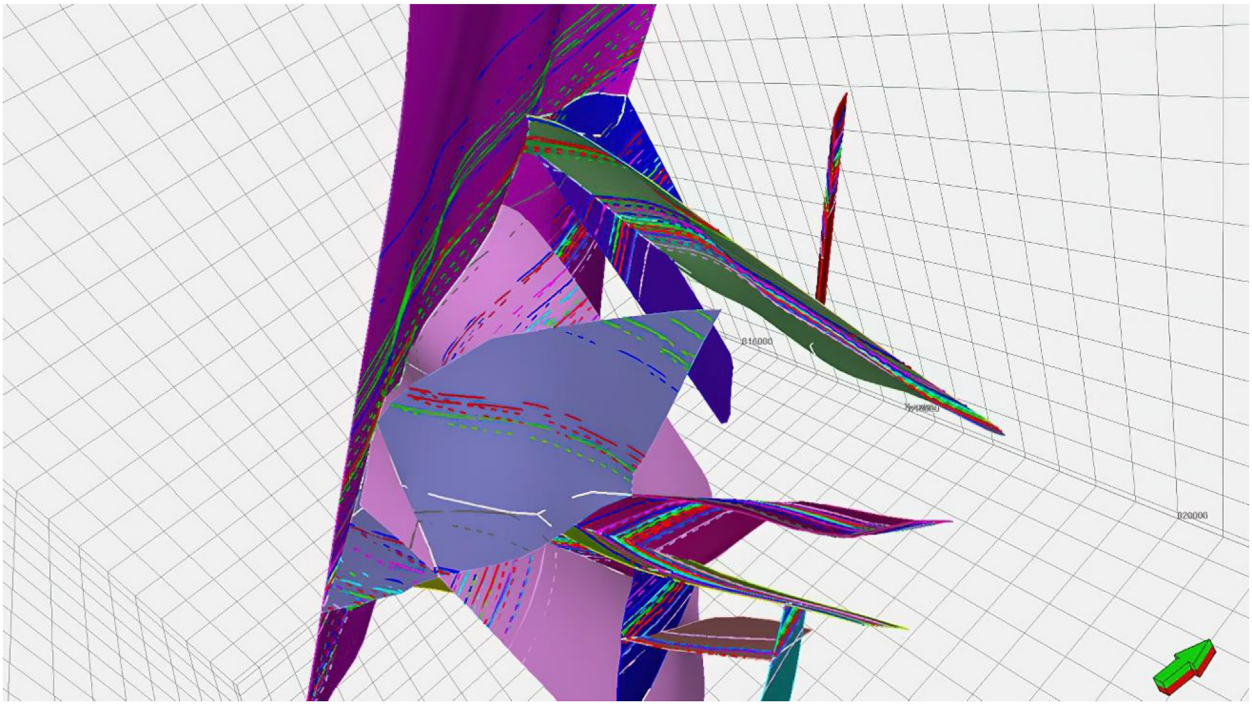

Fig. 9. The fault framework is displayed in a three dimensional window.

property simulations of reservoirs, and assessments of mineral resources (Yao, 2008; Liu et al., 2010).

4. Petrophysical analysis

A model usually comprises the facies model, porosity, permeability, and water saturation factors. Before the Well Logs upscaling facies and rock properties, estimations should be assigned to the well-supplied cells (Shepherd, 2009). Before moving forward with the model, the effects of scaled-up facies distribution and rock characteristics were explored to ensure that the important heterogeneities that influence flow were preserved.

The relationship between Gamma-ray magnitude and shale content may be linear or nonlinear. The relationships are all empirical (Islam et al., 2013).

Gamma-ray index, I_{GR}

$$I_{GR} = \frac{GR_{log} - GR_{min}}{GR_{Max} - GR_{Min}} \tag{3}$$

where,

I_{GR} Describes a linear response to shaliness or clay content.

GR_{log} = log reading at the depth of interest

GR_{clean} = gamma ray value in a nearby clean zone

GR_{shale} = gamma ray value in a nearby shale

Linear gamma ray - clay volume relationship:

$$V_{shale} = I_{gr}$$

Nonlinear gamma-ray - clay volume relationships: Steiber:

$$Steiber: V_{shale} = \frac{I_{gr}}{3.0 - 2.0\, I_{gr}} \tag{4}$$

To determine accurate porosity using a single porosity measurement, lithology must be identified (by selecting a matrix value). Lithology and porosity can be predicted [with considerable uncertainty] using two or more porosity measurements. The number of measurements enhances the complexity

Table 3. Litho-saturation analysis of wells.

Well	Zone	Top	Bottom	Gross	Net	Net to Gross (%)	Av- VSH (%)	Av- φ (%)	Av-S_w (%)
GS196-1A	MAT	11118.03	11479	16.098	1.943	12.3	12.3	21.7	46.1
OCT-A1ST1 (GS195-1ST1)	MAT	10935.92	11061.4	69.418	23.406	33.7	17.4	12.5	31.7
GS196-1A	NUBIA	12186.83	12235.3	22.562	2.25	10	10.4	15.1	64.7
OCT-A1ST1 (GS195-1ST1)	NUBIA	10009.78	10131.4	53.511	1.675	3.1	20.1	12.7	59.2

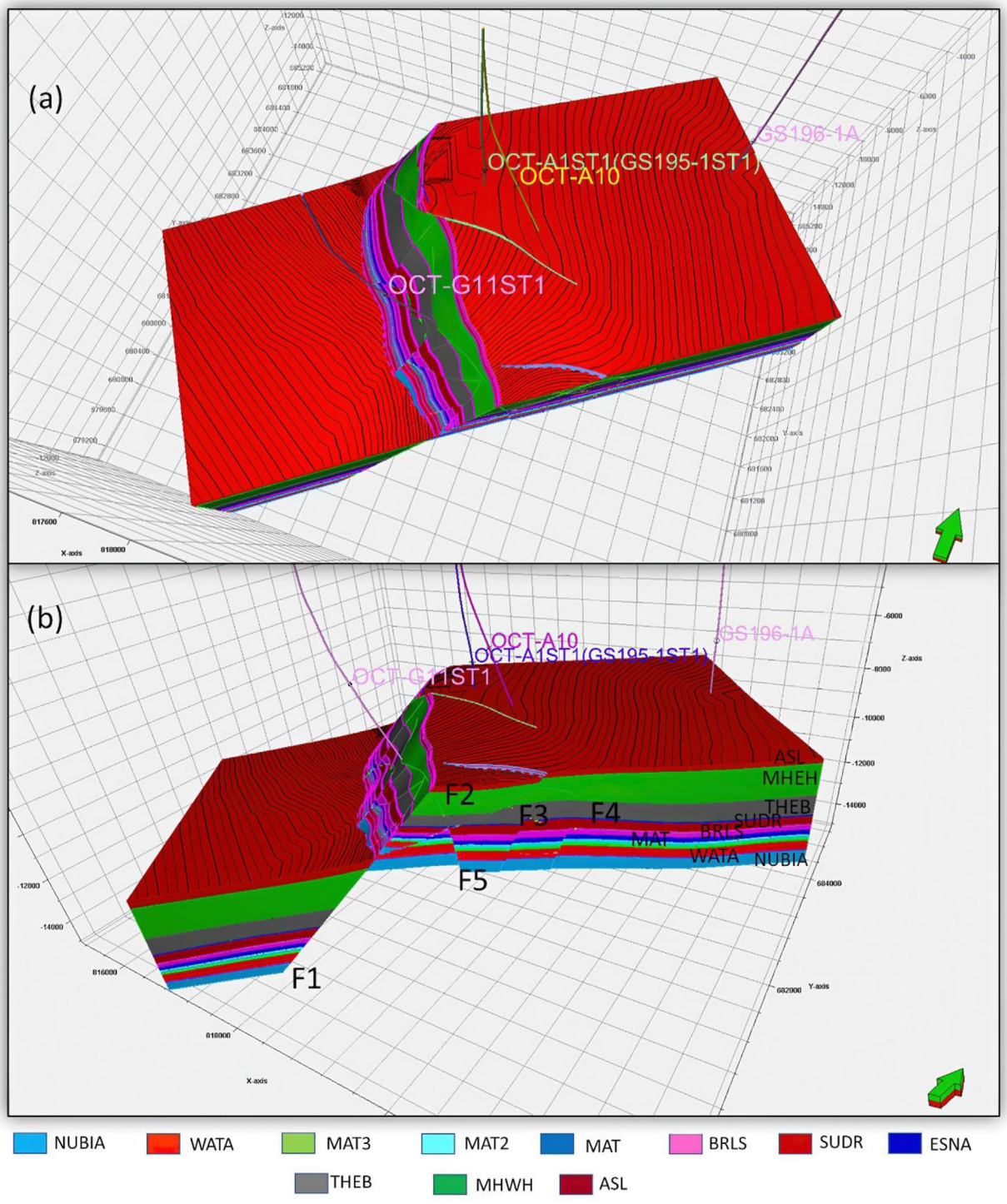

Fig. 10. (a) and (b) show the interpreted three dimensional structural model for the October oil field.

of the formation that can be postulated (Dolan, 1990).

$$D_{PHI} = \frac{\rho_{ma} - \rho_b}{\rho_{ma} - \rho_{fl}} \quad (5)$$

$D_{PHI} = \varnothing_D$ = density porosity.
ρ_b = bulk density (from the log).
ρ_{ma} = matrix density.
ρ_{fl} = fluid density (often assumed to be mud filtrate density).

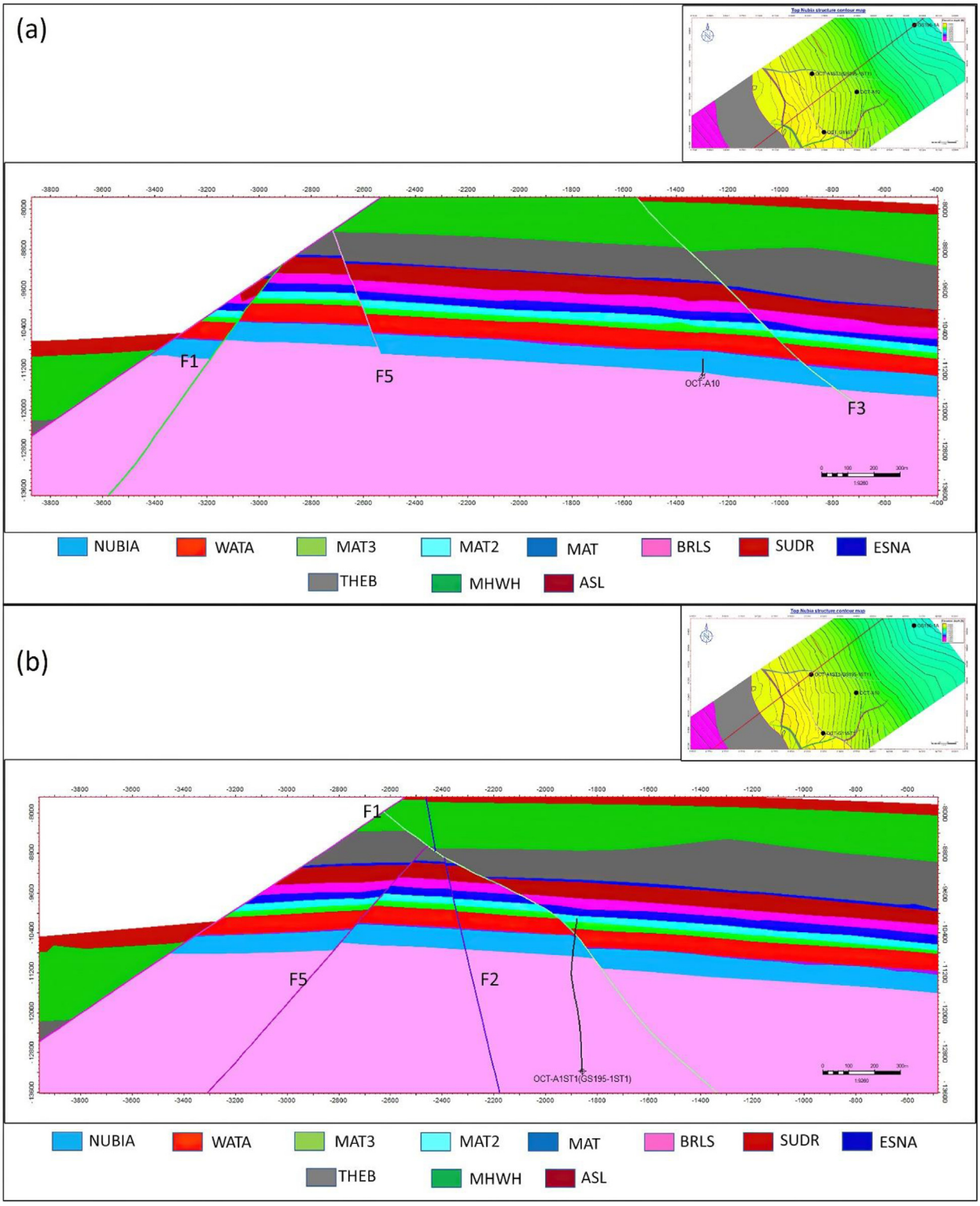

Fig. 11. (a) and (b) show two interpreted cross sections that illustrate the region is tectonically affected by a large normal fault (NE-SW) with large displacement followed by small normal and reverse faults.

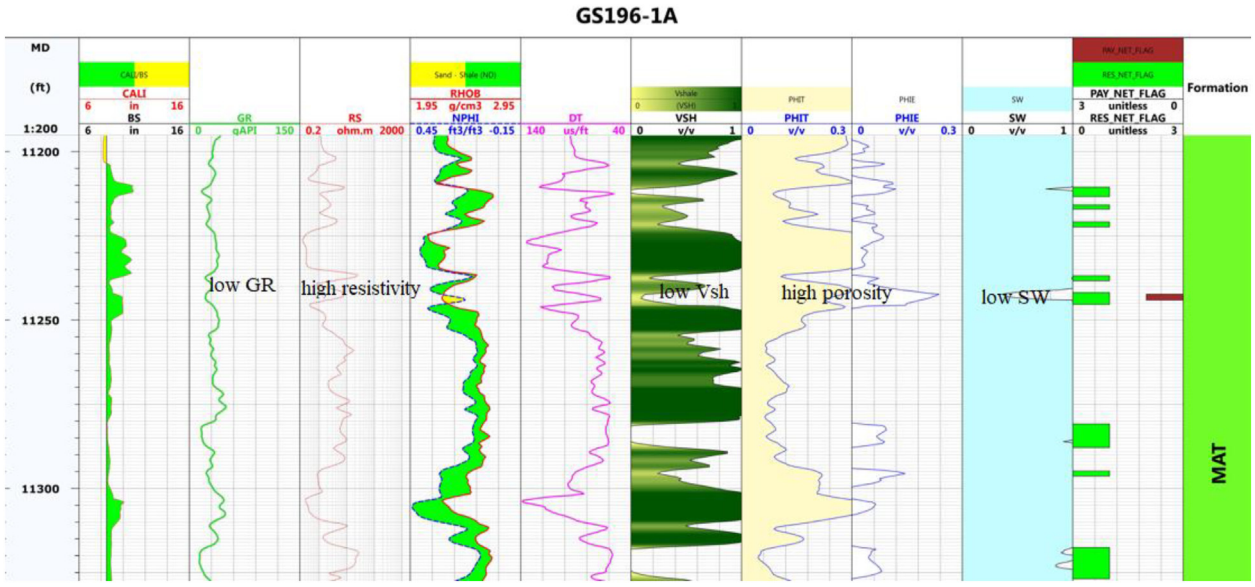

Fig. 12. Crossplot of MAT Formation at GS196-1A well, October field.

via Archie's Equation (Archie, 1942).

$$S_w = \left(\frac{a.R_w}{\varnothing^m.R_t}\right)^{\frac{1}{n}} \quad (6)$$

S_w = Formation water saturation.
R_w = Formation water resistivity.
R_t = True formation resistivity.
$\varnothing$ = Porosity.
a = cementation factor.
m = Cementation exponent.
n = saturation exponent.

5. Results

5.1. Facies modelling

The upscaled discrete facies' property appropriation is integrated into the 3D model via the facies demonstrating measure. This engagement began with a clear grasp of various lithologies as facies types, which were subsequently scaled up to model

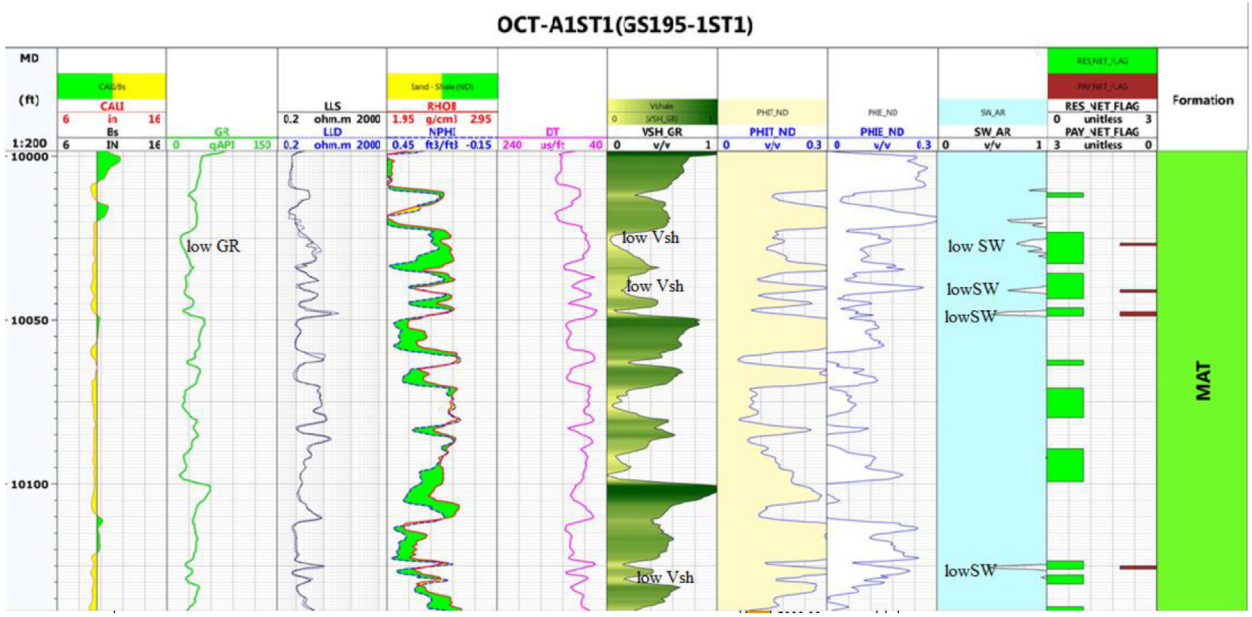

Fig. 13. Crossplot of MAT Formation at OCT-A1ST1 (GS195-1ST1) well, October field.

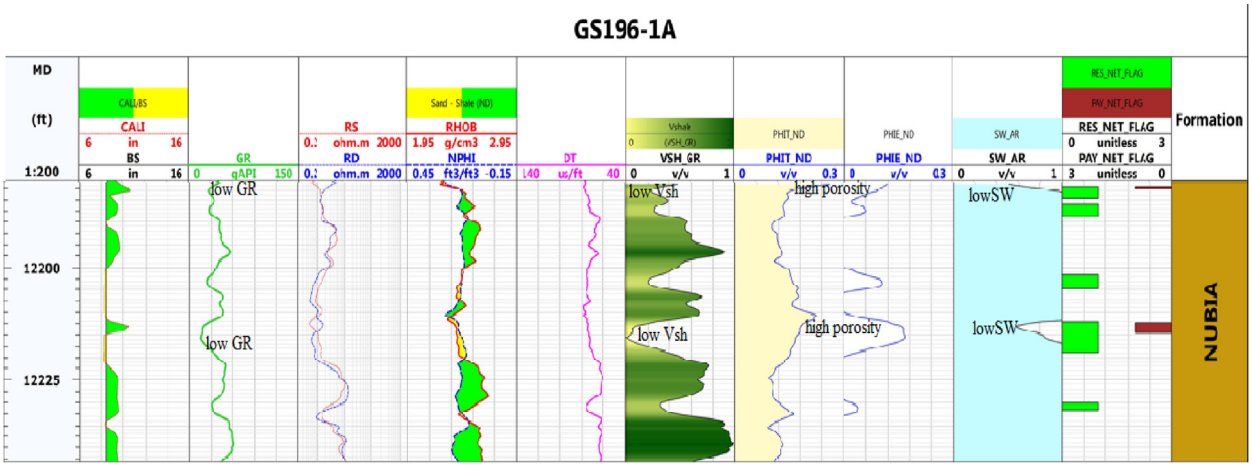

Fig. 14. Crossplot of NUBIA Formation at GS196-1A well, October field.

measurement as discrete characteristics or added to identify property patterns throughout the frame of the 3D model. Four wireline well records were used to distinguish between distinct facies log interpretations. Splitting the log of each analyzed reservoir surface into the four main lithologic facies, which are sandstone, limestone, shales, and anhydrite, allows us to examine the facies distribution.

5.2. Well logging analysis

The log analysis of MAT in GS196-1A, OCT-A1ST1 (GS195-1ST1) wells show that such wells have low gamma-ray values, high resistivity, and cross-over between the neutron and density responses, which indicate the presence of gas.

In GS196-1A well the top of MAT reservoir at 11,118.03 ft depth, with a gross thickness of 16.098 ft and a net-pay of 1.943. The well has V_{SH} of 12.3%, φ_E of 21.7%, and S_w of 46.1%. The top NUBIA reservoir is at 12,186.83 ft depth with a thickness of about 22.562 ft, a total net-pay of 2.25 ft, V_{SH} of 10.4%, φ_E of 15.1%, and S_w of 64.7%.

Matulla has low net pay, low effective porosity, low shale content, and low water saturation, while Nubia has the same characteristics but has high water saturation.

In the OCT-A1ST1 (GS195-1ST1) well the top of MAT reservoir at 10,935.92 ft depth, with a gross thickness of 69.418 ft and a net-pay of 23.406. The well has V_{SH} of 17.4%, φ_E of 12.5%, and S_w of 0.317%. The top NUBIA reservoir is at 10,009.78 ft depth with a thickness of about 53.511 ft, a total net-pay of 1.675 ft, V_{SH} of 20.1%, φ_E of 12.7%, and S_w of 59.2%. Matulla has high net pay, low effective porosity, low shale content, and low water saturation, while Nubia

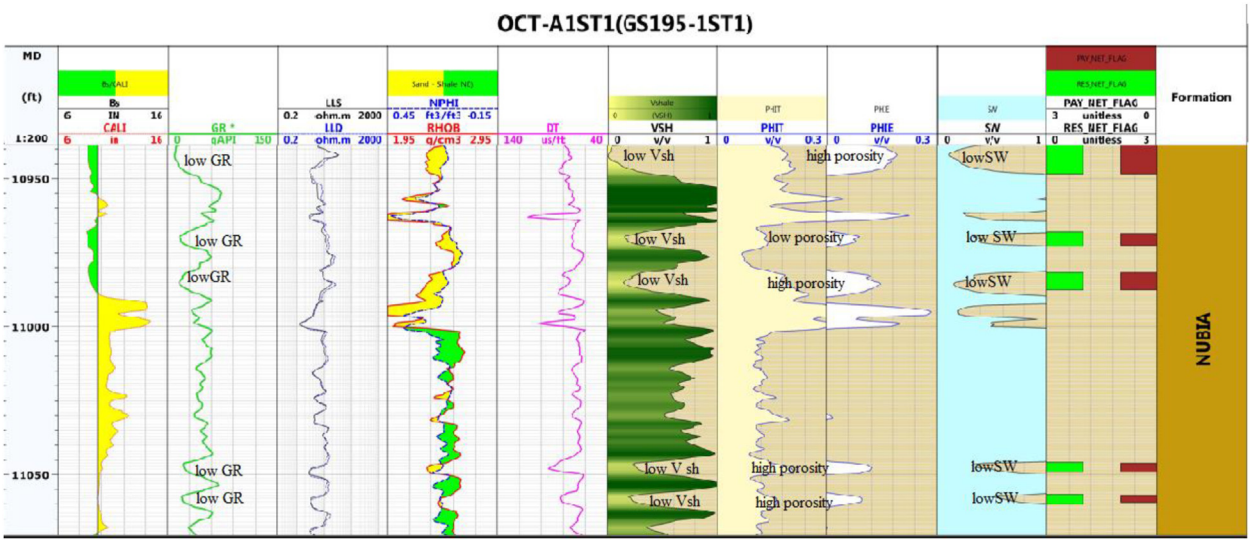

Fig. 15. Crossplot of NUBIA Formation at OCT-A1ST1 (GS195-1ST1) well, October field.

has low net pay, low effective porosity, low shale content, and high water saturation (Table 3).

5.3. 3D structural modeling

To comprehend the property distribution or heterogeneity of each reservoir surface, discrete properties from input well logs are loaded into the 3D static models built by the structural modeling workflow of the interpreted reservoir surfaces of the October seismic data (Fig. 8).

By using the previous steps illustrated in the workflow (Fig. 4) and extracting the skeleton grids in Fig. 9 to use it to generate the final 3D model created by the structural modeling workflow of the interpreted reservoir surfaces (Fig. 10). The region is tectonically affected by a large normal fault (NE-SW) with large displacement followed by small normal and reverse faults that may be the reason for the presence of traps. This structure is clear on the 3D structural model and cross sections (Fig. 11).

The extracted 3D structural model shows the fault's extension, location, and boundaries, which help define the best new prospect locations with better accuracy, and it revealed that the detailed 3D structural model supports the development plans (Figs. 9–10). In addition, Fig. 11 shows the fault planes far from the wells in the study area (OCT-A1ST1, GS195-1ST1, and OCT_A-10), which explains the low net pay from the log calculation.

6. Discussion and conclusion

Due to repeated tectonic movements, the October oil field in the Gulf of Suez, Egypt, comprises the primary components of hydrocarbon systems including shale source rock, sandstone reservoir formations, and the seal evaporite salt layers at various depths. Prior discoveries include very productive reservoir wells in the Lower Cretaceous Nubia and Matulla sandstone components (Figs. 13–15). The structural model and interpretations presented in this study, additional reservoir analysis, and petrophysical research on the lower and middle Miocene strata may lead to the discovery of new hydrocarbon accumulation sites. Numerous tectonic forces coming from different directions impact the tectonic regime in this region.

While the Rudeis Formation was being deposited in the early Miocene, the area was also susceptible to expansion and subsidence. Therefore, the faults and geological structures created by such extreme tectonics affect the process of hydrocarbon migration and accumulation in the area. According to the integration of the results from the subsurface geological data and reservoir models, two places are thought to be potential in MAT and NUBIA formation, one of these prospects is a fault and the other is a 3-way dip closure as depicted in Fig. 11.

By well-logging the litho-saturation analysis MAT in GS196-1A, OCT-A1ST1, and GS195-1ST1 wells show that such wells have low gamma-ray values, high resistivity, and a crossover between the neutron and density responses, which indicate the presence of gas. The October oil field had a lack of production in some places, which negatively impacted the economic value of this field, using saturation analysis in Table 3 and the 3D structural model gives precise results, especially for geological structures and the possibility of the presence of traps, which is clear from the model in Fig. 10. Utilising a 3D structural model in conjunction with well log data yields complementary results, including the fault size, boundaries, and location. Additionally, well data determine the facies, porosity, permeability, and water saturation parameters. The model reveals that the area lacks sufficient well coverage in the study area, and the existing wells have low net pay. Therefore, I recommend drilling new wells in the target formations along with the main geologic feature in this area. In F1, F2, F3, F4, and F5, these faults may be potential traps.

In conclusion, the study rock units, from the Zeit to the Nubia formations, are affected by distinct types of normal faults that follow NW-SE and NE-SW patterns. These faults play an important role in trap formation and hydrocarbon accumulation. The 3D reservoir modeling and petrophysical analysis of reservoir formations both show that the facies distribution of the chosen reservoir shifted from being predominately sandstone, shale, and limestone (NW) to being predominately limestone and sandstone (SE). The examined reservoir has favorable reservoir characteristics, which boost the production of hydrocarbon in this field (low net pay, low effective porosity, low shale content, and high water saturation). The structure set is thought to be in charge of the petrophysical findings and the facies distribution in the October oil field. The models demonstrate the effects of structural features and their control over the interpretation of the facies and petrophysical properties of reservoirs. The region is tectonically affected by a large normal fault (NE-SW) with large displacement, followed by small normal and reverse faults that may be the reason for the presence of traps. The extracted 3D structural model and cross-sections indicate faults in the region.

Conflicts of interest

There are no conflicts of interest.

Acknowledgment

The authors would like to express their gratitude to the Egyptian General Petroleum Corporation (EGPC) and PETROBEL (Belayim Petroleum) for providing the data needed to perform this work and giving permission to publish it. We also express our gratitude to the Fulbright Egypt Commission for awarding Dr. Amir Ismail the postdoctoral scholarship to Texas A and M University, Corpus Christi, enabling the completion of this research.

References

Abdel-Fattah, M., Gameel, M., Awad, S., & Ismaila, A. (2015). Seismic interpretation of the aptian Alamein dolomite in the razzak oil field, Western Desert, Egypt. *Arabian Journal of Geosciences*, 4669−4684.

Abdelwahhab, M. A., & Raef, A. (2020). Integrated reservoir and basin modeling in understanding the petroleum system and evaluating prospects: the Cenomanian reservoir, Bahariya Formation, at Falak Field, Shushan Basin, Western Desert, Egypt. *Journal of Petroleum Science & Engineering, 189*, Article 107023.

Archie, G. E. (1942). The electrical resistivity log as an aid in determining some reservoir characteristics. *Transactions of the AIME, 146*, 54−62.

Awni, F., A, R., M, A., & S, A. (1990). Belayim Marine and Belayim Land Oil Fields Structural Styles. EGPC, 10th Petrol. Expl. And Prod. Conf. In *10th Petroleum Exploration and Production Conference* (pp. 1−30). Cairo.

Badley, M. E. (1985). *Practical Seismic Interpretation*. Boston: IHRDC.

Badri, M. A., Taha, T. M., & Wiley, R. W. (1999). Subsalt Depth Imaging Using 3-D VSP Technique in the Ras El Ush Field, Gulf of Suez, Egypt. *GeoArabia, 4*, 363−378.

Chowdhary, L. R., & Taha, S. (1987). Geology and habitat of oil in Ras Budran field, Gulf of Suez, Egypt. *AAPG Bulletin, 71*, 1274−1293.

Dolan, P. (1990). Pakistan: a history of petroleum exploration and future potential. *Geological Society, London, Special Publications, 50*, 503−524.

EGPC. (1996). *Gulf of Suez oil fields (a comprehensive overview)* (p. 736). Cairo: Egyptian General Petroleum Corporation.

El Dally, N. H., Metwalli, F. I., & Ismail, A. (2023). Seismic modelling of the upper cretaceous, khalda oil field, shushan basin, western desert, Egypt. *Modeling Earth Systems and Environment, 9*, 4117−4134.

El Redini, N. A. H., Bakr, A. M. A., & Dahroug, S. M. (2017). Seismic data interpretation for hydrocarbon potential, for Safwa/Sabbar field, east Ghazalat onshore area, Abu Gharadig basin, Western Desert, Egypt. *NRIAG Journal of Astronomy and Geophysics, 6*, 287−299.

El Sawi, M. M. (1985). *Subsurface Studies on Area, Egypt (PhD thesis in Geology), Faculty of Science* (p. 261). El Mansoura University.

El-Gendy, N. H., El-Shishtawy, A., Barakat, M. K. H., & Shawaf, F. M. (2017). Applying sedimentological and geophysical techniques for facies analysis and depositional history of July Member sandstones, the northern area of July oilfield, Gulf of Suez, Egypt. *Journal of Applied Geology and Geophysics, 5*, 84−106.

El-Tarabili, E., & Adawy, N. (1972). Geologic history of the Nukhul-Baba area, Gulf of Suez,Egypt. *AAPG Bulletin, 56*, 882−902.

Farhoud, K. (2009). Accommodation zones and tectono-stratigraphy of the Gulf of Suez, Egypt: a contribution from aeromagnetic analysis. *GeoArabia, 14*, 139−162.

Gawad, E. A., Fathy, M., Reda, M., & Ewida, H. (2021). Petroleum geology: 3D reservoir modelling in the central Gulf of Suez, Egypt, to estimate the hydrocarbon possibility via petrophysical analysis and seismic data interpretation. *Geological Journal, 56*, 5329−5342.

Halbouty, M. T. (1992). Giant oil and gas fields of the decade 1978-1988. In *AAPG Conference-Giant Oil and Gas Fields of the Decade 1978-1988 Conference, September 9-12, (1990)*. Stavanger, Norway: American Association of petroleum geologists.

Hoffman, K. S., Neave, J. W., & Nilsen, E. H. (2006). Application of the fused fault block method in structural modeling and reservoir gridding of complex structures. In *SEG International Exposition and Annual Meeting* (pp. SEG−2006). SEG.

Islam, A., Habib, M., Islam, M., & Mita, M. (2013). Interpretation of wireline log data for reservoir characterization of the Rashidpur Gas Field, Bengal Basin. *Bangladesh, 1*, 47−54.

Ismail, A., Ewida, H. F., Al-Ibiary, M. G., Gammaldi, S., & Zollo, A. (2020a). Identification of gas zones and chimneys using seismic attributes analysis at the Scarab field, offshore, Nile Delta, Egypt. *Petroleum Research, 5*, 59−69.

Ismail, A., Ewida, H. F., Al-Ibiary, M. G., & Zollo, A. (2020b). Application of AVO attributes for gas channels identification, West offshore Nile Delta, Egypt. *Petroleum Research, 5*, 112−123.

Ismail, A., Radwan, A. A., Leila, M., Abdelmaksoud, A., & Ali, M. (2023). Unsupervised machine learning and multi-seismic attributes for fault and fracture network interpretation in the Kerry Field, Taranaki Basin, New Zealand. *Geomechanics and Geophysics for Geo-Energy and Geo-Resources, 9*, 122.

Khan, H. A., Zouaghi, T., Iftekhar, S., Khan, M. J., & Irfan, M. (2019). Plio-Pleistocene stratigraphic sequences and depositional model using 3D seismic interpretation constrained by well logs in Central Graben, North Sea. *J Earth Syience, 128*, 1−19.

Khattab, M. A., Radwan, A. E., El-Anbaawy, M. I., Mansour, M. H., & El-Tehiwy, A. A. (2023). Three-dimensional structural modelling of structurally complex hydrocarbon reservoir in October Oil Field, Gulf of Suez, Egypt. *Geological Journal, 58*, 4146−4164.

Lelek, J. J., Shepherd, D. B., Stone, D. M., & Abdine, A. S. (1992). *October field: The latest Giant under development in Egypt's Gulf of Suez: Chapter 15*.

Liu, S., Xiao, K., & Wang, X. (2010). Three-dimensional geological property model and its visualization. *Geological Bulletin of China, 29*, 1554−1557.

Montenat, C., Ott D'Estevou, P., & Purser, B. H. (1998). The Suez Rift and the North-westernRed Sea Neogene sedimentation and tectonic evolution. In *Dynamics and Methods of study of Sedimentary Basins* (pp. 173−199). Editions Technip (English edition, Oxford and IBH Publishing.

Moustafa, A. R., & Khalil, S. M. (2020). Structural Setting and Tectonic Evolution of the Gulf of Suez, NW Red Sea and Gulf of Aqaba Rift Systems. In *The Geology of Egypt* (pp. 295−342). Cham: Springer.

Patton, T. L., Moustaffa, A. R., Nelson, R. A., & Abdine, S. A. (1994). *Tectonic evolution andstratigraphic setting of the Suez rift*. In S. A. London (Ed.) (vol. 59, pp. 7−55). Interior Rift Basins. AAPG Mem.

Paulsson, Björn, Fuller, B., Karrenbach, M., & Heuermann, F. (2001). Borehole data: closer to the rocks. *Explorer, 22*, 7.

Radwan, A. E., Husinec, A., Benjumea, B., Kassem, A. A., Abd El Aal, A. K., Hakimi, M. H., & Shehata, A. A. (2022). Diagenetic overprint on porosity and permeability of a combined conventional-unconventional reservoir: Insights from the Eocene pelagic limestones, Gulf of Suez, Egypt. *Marine and Petroleum Geology, 146*, Article 105967.

Sercombe, W. J., Thurmon, L., & Morse, J. (2012). Advanced reservoir modeling in poor seismic, October Field, northern Gulf of Suez, Egypt. In *AAPG International Conference and Exhibition, Milan, Oct* (pp. 23−26).

Shepherd, M. (2009). Oil Field production geology. In *AAPG Memoir 91*. Oklahoma: The American Association of Petroleum Geologists.

Thom, J., & Hocker, C. (2009). 3-D grid types in geomodeling and simulation—how the choice of the model container determines modeling results. In *Proceedings of the AAPG Annual Convention and Exhibition. Denver, Colorado, USA*.

Yao, L. (2008). *Research on Three-Dimensional Property Modeling Method Based on Geostatistics*. Beijing, China: Peking University.

Zahra, H. S., & Nakhla, A. M. (2016). Tectonic and structural setting of the northeastern central Gulf of Suez area using aeromagnetic data. *Journal of African Earth Sciences, 115*, 1−16.

Zahran, M. E. (1986). Geology of the October oilfield. In *Proc. EGPC 8th Expl. Conf* (pp. 52−53).

Zouaghi, T., Ferhi, I., Bédir, M., Youssef, M. B., Gasmi, M., & Inoubli, M. H. (2011). Analysis of Cretaceous (Aptian) strata in central Tunisia, using 2D seismic data and well logs. *Journal of African Earth Sciences, 61*, 38−61.